iScience

CellPress
OPEN ACCESS

Review

Two-dimensional materials and their applications in fuel cells

Zeyu Lu,[1] Erbo Zhao,[1] Chao Zhang,[2,*] and Chen Chen[1,*]

SUMMARY

In recent years, two-dimensional (2D) materials have been extensively studied and applied in the field of catalysis on account of their high specific surface areas, high exposure of metal active sites, and readily tunable structures. This article introduces various 2D materials (including materials composed of a few atomic layers) and the related synthesis methods and discusses their catalytic performances for hydrogen fuel cells, in particular, for oxygen reduction reaction and hydrogen oxidation reaction. At the end of this review, the advantages and current challenges of 2D materials are summarized, and the prospects of 2D electrocatalytic materials are proposed.

INTRODUCTION

In the past few centuries, fossil fuels have been the most important energy source for the human society. However, the overdependence on fossil energy and the resulting environmental problems urge people to develop more efficient and eco-friendly means for energy utilization.[1,2] In this regard, electrochemical conversion is generally considered one of the most promising approaches and has been studied extensively, as it features high energy conversion efficiencies and the extra advantage of controlling the reaction kinetics by adjusting the potential/voltage.

Electrochemical cells play a very important role in the field of new energy. In order to utilize fossil fuels more efficiently, fuel cells have been under intense scrutiny. Compared with thermal engines, fuel cells have the advantages of high energy efficiency, low pollution, and minimal noise during operation.

For electrochemical cells, the electrode materials are probably the most important components, as the electrocatalytic reactions take place at the electrode/electrolyte interface. Typically, catalytic materials have transition metals (such as Ni,[3] Pt,[4] and Ag[5]) as the active species to participate in reactions, and precious metals are often used in these catalysts because of the excellent coordinating ability of their *d* orbitals. However, the stability of these catalysts yet needs to be improved, and their high cost constrains their commercialization.[1] During the reaction process, the atoms at the interiors of these metal particles are inaccessible to the reactant molecules. Therefore, loading metal particles on a support with a higher specific surface area and minimizing the particle sizes are effective ways to lower the metal usage.

In this regard, two-dimensional (2D) materials could ideally serve as support for electrocatalysts. They have a number of advantages: (1) high surface areas, which could help to accommodate a larger number of metal particles; (2) readily modifiable surfaces, which could lead to a proper interaction between metal and support; (3) excellent mechanical strength and flexibility, which could allow for fabricating flexible films in functional devices. Since the first report on graphene in 2004,[6] various 2D materials have emerged and been studied (such as MXenes,[7] g-C_3N_4,[8] transition metal dichalcogenides [TMDs],[9] layered metal hydroxides [LMHs][10]). In the field of electrocatalysis, most of the pristine 2D materials inherently have inferior catalytic performances; for example, graphene has a poor ability to adsorb hydrogen, and g-C_3N_4 has low electrical conductivity, resulting in poor electrocatalytic performance in hydrogen evolution reaction (HER).[11] In practice, the catalytic activities of 2D materials are often improved by doping foreign atoms (metal atoms, in particular). This article will introduce a few most representative 2D materials and discuss the catalytic materials suited for different electrode reactions.

TWO-DIMENSIONAL MATERIALS

Graphene

In 2004, K. S. Novoselov and A. K. Geim prepared single-layer graphene using the micromechanical exfoliation method.[12] Such structures had previously been considered impossible to exist, because in the 1940s, Landau and Peierls' theory predicted that strictly 2D crystals would be thermodynamically unstable.[13] The discovery by Novoselov and Geim sparked a strong interest in this "impossible" material among the

[1]Department of Chemistry, Tsinghua University, Beijing 100084, China
[2]MOE International Joint Laboratory of Materials Microstructure, Institute for New Energy Materials and Low-Carbon Technologies, School of Materials Science and Engineering, Tianjin University of Technology, Tianjin 300384, China
*Correspondence: czhang@email.tjut.edu.cn (C.Z.), cchen@tsinghua.edu.cn (C.C.)
https://doi.org/10.1016/j.isci.2024.109841

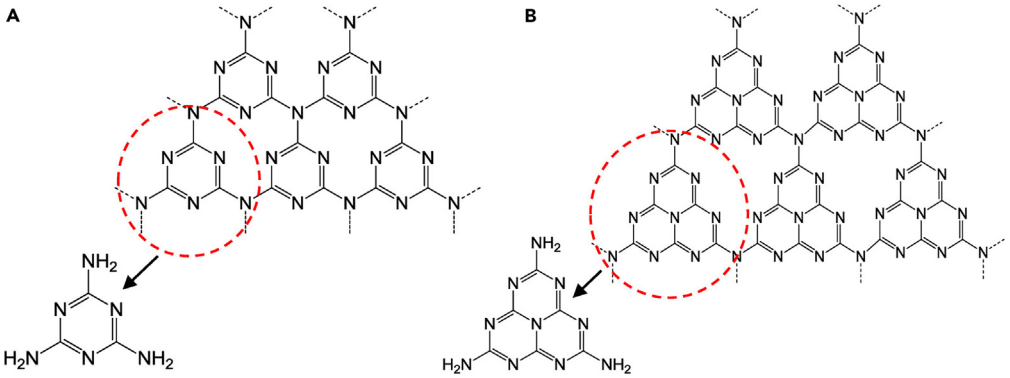

Figure 1. The structure models of g-C_3N_4

(A) s-Triazine.

(B) Tri-s-triazine. Reprinted with permission from ref. [8]. Copyright 2016 American Chemical Society.

scientific communities. Now it has been found that graphene has a number of outstanding physical properties: a large theoretical surface area (up to 2,630 m^2 g^{-1}),[14] an ultrahigh electrical conductivity (106 S cm^{-1}),[15] and an excellent mechanical strength. For unmodified graphene, owing to the presence of delocalized π bonds within its layer, the surface energy is relatively low, which is not conducive to the adsorption of reaction intermediates; therefore, unmodified graphene shows relatively low electrocatalytic activities.[16] However, the high specific surface area qualifies graphene as a good support for loading metal particles and dopant atoms. For example, Xia et al. synthesized a series of high-loading M–N_4-doped graphene materials via graphene quantum dot crosslinking and self-assembly for CO_2 reduction reaction.[17]

Graphitic carbon nitride

Graphitic carbon nitride (g-C_3N_4) is a layered 2D material and is considered the most stable C–N compound.[8] Figure 1 shows two typical structural arrangements of g-C_3N_4. The structure model in Figure 1A features a cyclic arrangement of triazine rings with carbon vacancies, and the model in Figure 1B features triazine subunits fused via planar tertiary amines.

g-C_3N_4 can also be used as a support material in electrocatalysis, and to improve the electrical conductivity, it is usually hybridized with conductive carbon materials.[18] Ma et al. reported a phosphorus-doped g-C_3N_4 material for flexible oxygen electrodes, which can serve as the cathode for Zn–air batteries.[19]

Transition metal dichalcogenides

The general formula for layered transition metal dichalcogenides (TMDs) could be denoted as MX_2 (where M is a transition metal, and X is a chalcogen element). As shown in Figure 2A, there are approximately 40 types of layered TMDs, some of which have been used to catalyze electrochemical reactions such as hydrogen evolution reaction. In addition, it has been confirmed that the edge of the layers is the active site featuring lower adsorption Gibbs free energy.[20]

Layered transition metal oxides and hydroxides

Transition metal oxides (TMOs) and hydroxides (TMHs) are widely used in the field of electrocatalysis. The structure of layered TMOs is similar to that of graphite, and the corresponding synthesis method is also similar to that of TMDs.[22] Owing to the low catalytic activity and poor electrical conductivity of pristine TMOs and TMHs, their electrocatalytic performances are far from ideal. Increasing surface oxygen vacancies is an effective way to elevate the catalytic performance. For example, Wang et al. synthesized Co_3O_4 nanosheets by plasma engraving, which improves the conductivity and endow the nanosheets with activity for oxygen evolution reaction.[23]

Layered TMHs can be classified into layered single-metal hydroxides (LSHs) and layered double-metal hydroxides (LDHs). Their main structure is a metal hydroxyl base layer similar to that of brucite and may be positively charged on account of the metal cations with different types or valence states. Each metal ion occupies the center of an octahedron composed of six hydroxyl ions, and different hydroxyl octahedra are connected into a planar structure in a co-edge manner (Figure 3).[10]

The interlayer region of LDHs is occupied with anions and other metal cations, and the chemical properties can be controlled by adjusting these components. For example, Qian et al. synthesized a Ni-Co-Fe ternary LDH, which exhibits good dual functional performance for ORR and OER (oxygen evolution reaction).[24]

MXenes

In 2011, Naguib et al. discovered and studied a new type of 2D nanomaterial and named it "MXene." The first materials ever discovered have a general chemical formula $Ti_3C_2X_2$ ($X = F^-$, OH^-) and were prepared by separating the Ti_3C_2 layer by selectively etching Al in

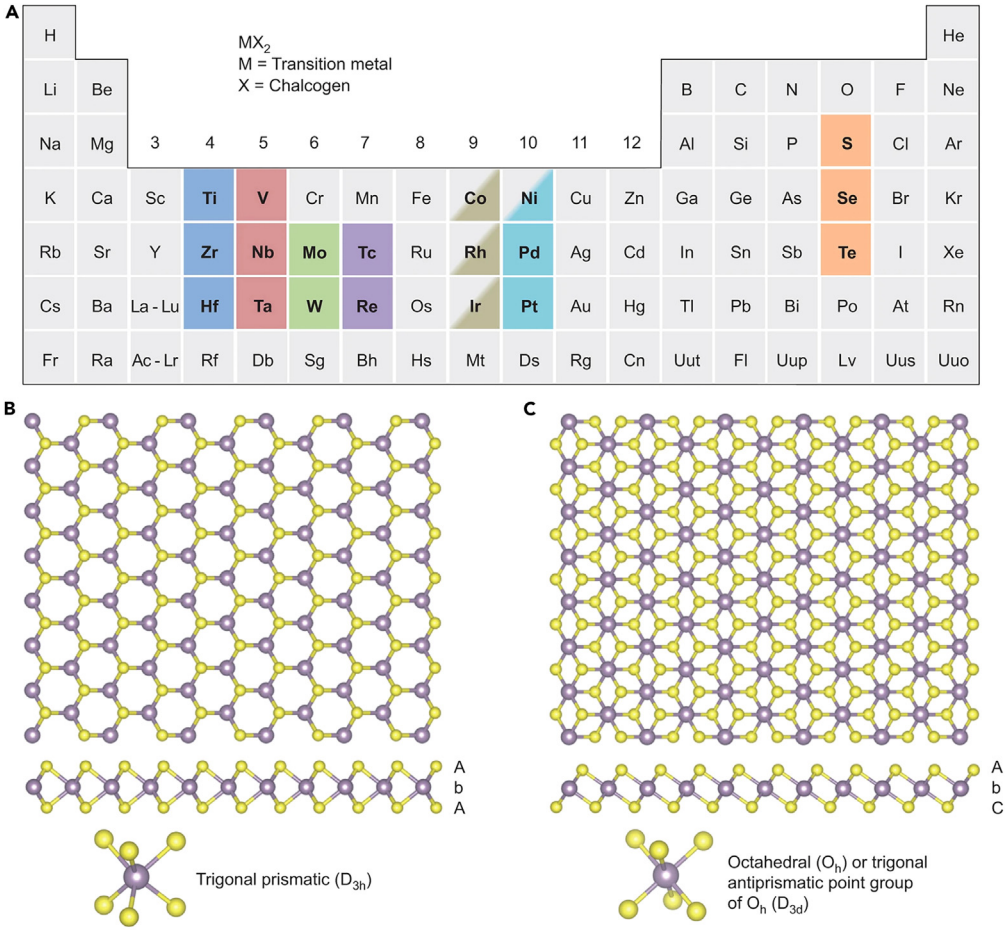

Figure 2. Elemental composition and structure of layered dichalcogenides

(A) Chalcogen elements and metallic elements with which layered crystals can be formed are highlighted in the table. Partial highlighting indicates that only some of the dichalcogenides are layered.

(B and C) Structural illustration of single-layer TMD with triagonal prismatic (B) and octahedral (C) coordinations. Atom color code: purple, metal; yellow, chalcogen. Reprinted with permission from ref.[21]. Copyright 2013 Springer Nature.

Ti_3AlC_2.[25] Thus far, many types of MXenes have been synthesized or predicted, and their common formula can be denoted as $M_{n+1}AX_n$, where M represents an early transition metal, A is a 13- or 14-group element, and X is C or N.[26] Figure 4 shows the structure and elemental composition of MXexes.

These materials usually have good electrical conductivity and hydrophilicity, which qualifies them as suitable raw materials for electrocatalysis. However, the catalytic activities of the pristine MXenes are rather low, and therefore, MXenes are usually used as support for the catalyst. For example, in 2018, Zhang et al. reported a double-transition metal MXene nanosheet (Mo_2TiCT_x) supporting Pt single atoms for hydrogen evolution reaction (HER).[27]

Xenes

Xenes are mono-elemental layered materials, which mainly include elements in Group IVA, V, and IIIA, such as phosphorene,[28] arsenene, and bismuthene. They have unique physical properties for their ultrathin 2D structures.[29] And they are suitable to be support for single-atom materials.[30] Some emerging Xenes have been demonstrated to show potential in electrocatalysis, such as bismuthene[31] and selenene.[32]

2D metal–organic frameworks

Metal–organic frameworks (MOFs) are porous crystals connected by organic ligands and various metal centers, typically featuring a high specific surface area, adjustable structures, and pore channels and could potentially be used as electrocatalytic materials.[33] Moreover, 2D MOFs can be obtained by exfoliating or growth, like other 2D nanomaterials.[34–36] For example, Zhao et al. synthesized NiCo bimetallic

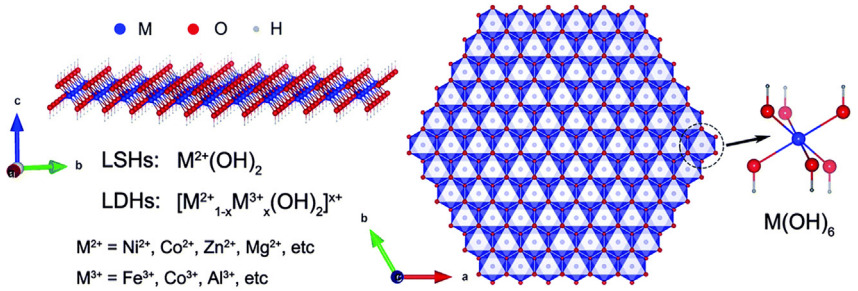

Figure 3. Schematic illustration of single-layer structure of LSHs and LDHs
Reprinted with permission from ref. [10]. Copyright 2012 Royal Society of Chemistry.

organic framework nanosheets and used them for OER.[34] The ultra-thin thickness of this material and the coordination-unsaturated metal atoms confer a high catalytic activity. Another advantage of 2D MOFs lies in the convenience of anchoring single atoms. For example, Chen et al. prepared Fe single atoms using the coordination of N atoms in the molecular cage of ZIF-8, which showed a good performance for ORR.[37]

Metals and alloys

Most metals crystallize in three ways: face-centered cubic (fcc), hexagonal close-packed (hcp), or body-centered cubic (bcc). For fcc and hcp structures, the bulk materials could be considered to be composed of 2D dense layers, and 2D metals have the same structure with that of bulk metals. If some atoms are replaced with other metal atoms, the resulting alloys have similar crystal structures to that of pristine metals, but they could display quite different catalytic activities. Alloys with heterostructures used for electrochemistry have also been reported.[38]

SYNTHESIS OF 2D MATERIALS

Thus far, a range of methods have been developed for preparing 2D materials, which can be generally divided into top-down methods and bottom-up methods. Top-down methods here refer to the detachment of 2D layered crystals from their parent crystals, such as mechanical exfoliation and liquid exfoliation. Bottom-up methods refer to the direct synthesis of target 2D materials from precursors, such as chemical vapor deposition and wet chemical methods.

Mechanical exfoliation

The mechanical exfoliation method refers to exfoliating by applying force between layers. As the interlayer interactions of layered 2D materials are much weaker than the intralayer ones, the layered structure could be largely preserved. This method has been widely known for successfully separating monolayer graphene from graphite[12] and later proved to be suitable for the separation of other layered crystals.[39] This separation process does not require chemical reactions, and therefore, the obtained 2D materials generally feature clean surfaces and large lateral sizes. However, the production rate of this method is rather low, and the thickness of the separated samples is not uniform, which limits their application.

Liquid exfoliation

Similar to mechanical exfoliation, the essence of liquid exfoliation is to apply force between layers to separate them. By soaking bulk crystals in a suitable solvent and using ultrasound to assist in peeling, 2D materials can be rapidly obtained.

For ultrasonic-assisted exfoliation in solvents, solvents with proper surface energy are required for different bulk crystals. Alternatively, the surface tension of the solvent can be adjusted by adding surfactants. This method is widely used for various layered compounds, but it still has a few drawbacks: (1) single-layer nanosheets could hardly be peeled off; (2) the lateral size of the nanosheets is usually small; (3) there may be residual surfactants adsorbed on the 2D nanosheets; (4) some defects may be introduced on the nanosheets during the peeling process. These drawbacks can affect the catalytic performance of the resulting materials.

Another method is ion-intercalation-assisted liquid exfoliation, which involves intercalating metal cations (Li^+, Na^+, K^+, etc.) into the interlayer spaces of bulk metal sulfide crystals, further weakening the interlayer interaction and achieving exfoliation. For example, by refluxing the bulk crystals in a butane solution of *n*-butyl lithium for a few days, the bulk crystals could form lithium intercalation compounds, which are then transferred into aqueous phase for further ultrasonication. During this process, the lithium intercalation compounds would react with water to produce hydrogen gas, promoting the detachment process.[39] This method requires a longer time for lithium insertion and uses dangerous metal–organic compounds that are highly sensitive to water and oxygen.

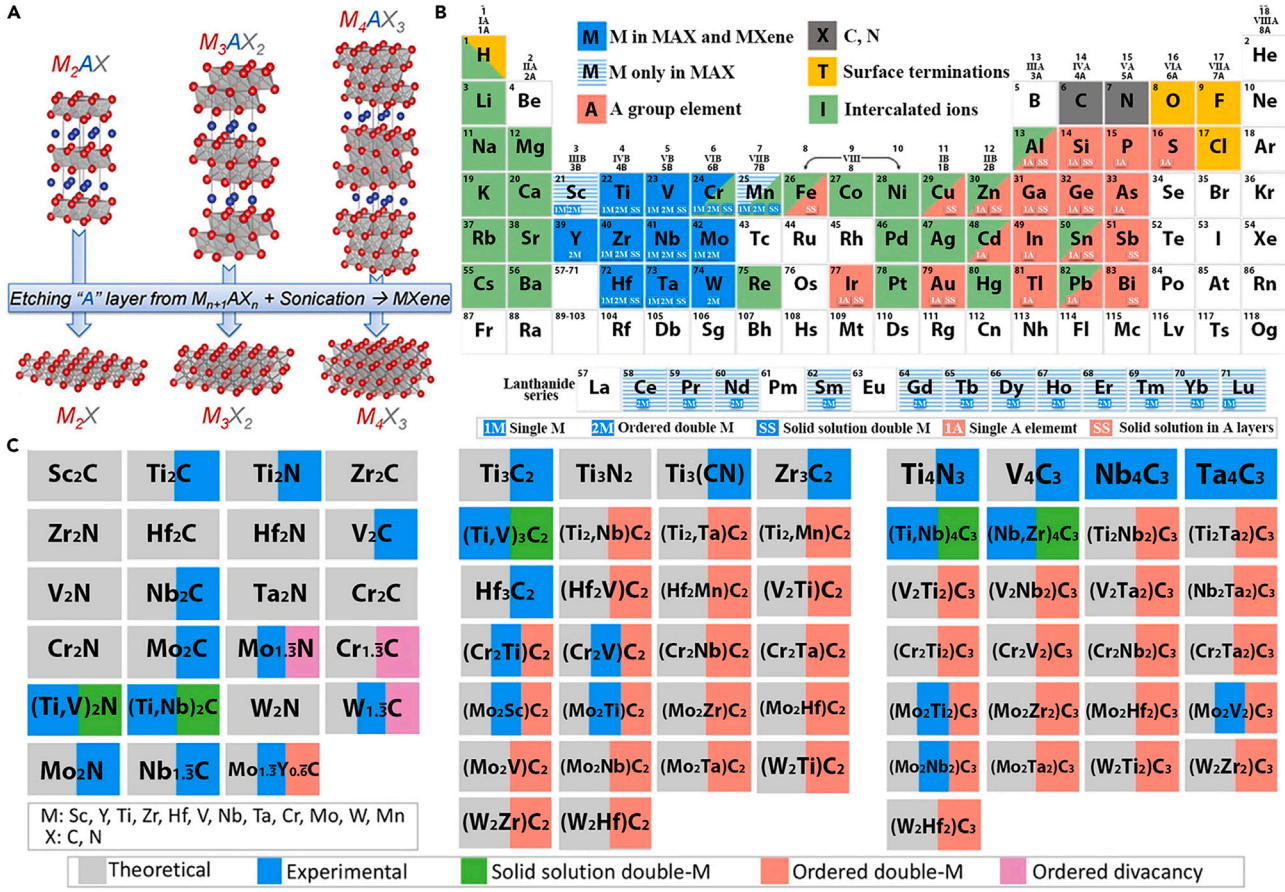

Figure 4. The structure and elemental composition of reported MXene

(A) Schematic illustration of pristine MXenes and MAX phases.

(B) Elemental composition of MAX phases and MXenes.

(C) MXene compositions reported to date. Reprinted with permission from ref. [26]. Copyright 2020 American Chemical Society.

Chemical vapor deposition

The chemical vapor deposition (CVD) method was initially applied to produce high-purity films such as W, Ti, and Si films. With the development of this method, it gradually became applicable to various types of materials, such as graphene. In this method, the substrate is placed in a furnace chamber, and the gases are circulated into the furnace chamber. These gases react therein, and the reaction products are deposited on the substrate surface. In 2009, Pollard et al. reported the work of using the CVD method to grow single-layer graphene on the SiO_2/Si surface deposited by Ni. Here, Ni acts as both a substrate and a catalyst for the formation of graphene.[40]

Solvothermal synthesis

Solvothermal synthesis is a common wet chemical synthesis method used in the synthesis of various materials. This method heats the solvent in a closed container, causing the raw material to react at a temperature higher than the standard boiling point of the solvent to improve the reaction rate and crystallinity. This method is also widely used in the synthesis of 2D materials. For example, Dou et al. developed a general strategy for synthesizing TMOs and synthesized 2–7 atomic thick TMO nanosheets.[41] However, the reaction mechanism of the solvothermal synthesis is difficult to explore, and the reaction is highly sensitive to the experimental conditions, which makes it difficult to design synthesis methods for different material systems. Moreover, most 2D nanosheets synthesized in this way are multi-layered.

Self-assembly

With the advance of nanocrystal synthesis technologies, the method of fabricating 2D nanomaterials via self-assembly has been developed. In such a process, nanocrystals coalesce together through non-covalent interactions such as hydrogen bonding or van der Waals forces, resulting in 2D crystals with larger lateral dimensions. In 2006, Tang et al. first prepared CdTe nanosheets from CdTe nanocrystals by self-assembly.[42] This method can also help to load metal atoms onto 2D supports.[43]

Table 1. Summary of ORR performance for some reported materials

Catalysts	$E_{1/2}$ (V vs. RHE)	j_L (mA cm^{-2})	Reference
rGO@mC-Co-850	0.82	5.97	Qiu et al.[43]
Ag–Fe–C/N	0.87	4.43	Lai et al.[5]
MCCF/NiMn-MOFs	0.73	5.60	Cheng et al.[44]
FeCo/NPC	0.81	4.85	Gao et al.[45]
FeCo-NC_{ps}	0.85	5.73	Liu et al.[46]

ELECTRODE REACTIONS IN FUEL CELLS AND RELEVANT MATERIALS

Fuel cells have the advantages of high energy conversion, low noise, and minimal carbon emission, which can be widely used in automobiles, trains, fixed power stations, etc. According to the electrolyte used, fuel cells are classified into the following different types: alkaline fuel cell (AFC), phosphoric acid fuel cell (PAFC), proton-exchange membrane fuel cell (PEMFC), solid oxide fuel cell (SOFC), and molten carbonate fuel cell (MCFC).

The two electrode reactions are the oxidation of fuel at the anode and the reduction of oxygen at the cathode. Here, we will introduce these two reactions separately. Tables 1 and 2 summarize some materials that have been applied in ORR and HOR.

Oxygen reduction reaction

Reaction mechanism

Oxygen reduction reaction (ORR) in aqueous solution may undergo two pathways: (1) O_2 is directly reduced to H_2O or OH^- through the $4e^-$ pathway; (2) O_2 is first reduced to H_2O_2 or HO_2^- through the $2e^-$ pathway, and then H_2O or OH^- is generated through the one-step $2e^-$ pathway. The corresponding reaction equations are listed below[51]:

(1-1) Dissociative

$$O_2 + 2* \rightarrow 2O_{(ads)} \quad \text{(Equation 1)}$$

$$O_{(ads)} + H_2O + e^- \rightarrow OH_{(ads)} + OH^- \quad \text{(Equation 2)}$$

$$OH_{(ads)} + e^- \rightarrow OH^- \quad \text{(Equation 3)}$$

(1-2) Associative

$$O_2 + * \rightarrow O_{2(ads)} \quad \text{(Equation 4)}$$

$$O_{2(ads)} + H_2O + e^- \rightarrow OOH_{(ads)} + OH^- \quad \text{(Equation 5)}$$

$$OOH_{(ads)} + e^- \rightarrow O_{(ads)} + OH^- \quad \text{(Equation 6)}$$

Followed by steps (2) and (3).

(2-2) Instead of (6), $OOH_{(ads)}$ desorbs

$$OOH_{(ads)} + e^- \rightarrow OOH^- \quad \text{(Equation 7)}$$

In fuel cells, the first pathway is preferred as it can provide higher current efficiency. The pathway of this reaction mainly depends on the adsorption energy of oxygen.[51] For example, the adsorption energy on the carbon surface is quite high, which is not conducive to the

Table 2. Summary of HOR performance for some reported platinum-group-metal-based materials

Catalysts	Mass activity (A mg_{PGM}^{-1})	Reference
RhMo NSs	6.96	Zhang et al.[38]
$Pt_{0.1}Ru_{0.9}$	1.9	Strmcnik et al.[47]
Pt_6NCs/C	3.658	Wang et al.[48]
i-ZnIn-PR/C	10.2	Huang et al.[49]
Pt/NiO-300	2.86	Zhao et al.[50]

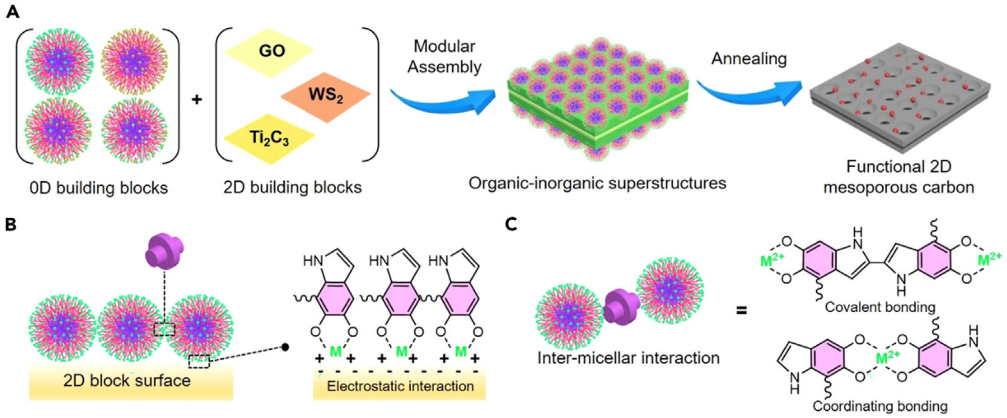

Figure 5. Schematic illustration of 2D mesoporous material synthesis and interaction

(A) MC/PS-b-PEO single-micelle building blocks self-assembly diagram.

(B) Schematic illustration of the interaction between the MC/PS-b-PEO with the 2D surfaces.

(C) Schematic illustration of the inter-micelle interactions. Reprinted with permission from ref. [43]. Copyright 2023 Springer Nature.

$4e^-$ process and favors the $2e^-$ process.[52] In contrast, oxygen has a strong tendency of dissociation on metal surfaces (such as Pt), and the $4e^-$ pathway is favored.

Measurement

Usually, steady-state polarization on a rotating disk electrode (RDE) or a rotating ring disk electrode (RRDE) is used to assess the ORR activity. Metrics for performance assessment such as onset potential, half-wave potential ($E_{1/2}$), and limit current density (j_d) could be obtained via linear sweep voltammetry (LSV). The ORR current can be expressed using the Koutchy–Levich (K–L) equation:

$$\frac{1}{j} = \frac{1}{j_k} + \frac{1}{j_d} \quad \text{(Equation 8)}$$

where j is the total current, j_k is the kinetic control current, and j_d is the limit current. j_k can be regarded as a constant, and j_d can be expressed by the following equation:

$$j_d = 0.620nFAC_0D^{2/3}\omega^{1/2}\nu^{-1/6} \quad \text{(Equation 9)}$$

in which n is the number of transferred electrons, F is the Faraday constant, A is the electrode area, C_0 is the oxygen concentration in the solution, D is the oxygen molecular diffusivity, ω is the RDE rotational speed, and ν is the kinematic viscosity of the solution.

$$\text{Let } K = 0.620nFAC_0D^{2/3}\nu^{-1/6} \quad \text{(Equation 10)}$$

And then the K–L equation can be expressed as

$$\frac{1}{j} = \frac{1}{j_k} + \frac{1}{K}\frac{1}{\omega^{1/2}} \quad \text{(Equation 11)}$$

Then, on the basis of different rotational speeds and corresponding current densities under the same voltage, the slope of the fitted straight line can be used to calculate the total electron transfer number n.

Metal-loaded reduced graphene oxide

For graphene derivatives, reduced graphene oxide (rGO) has rich defects that can be used to anchor metal particles. Qiu et al. synthesized highly uniform metal catecholamine complexes, which can easily connect to the 2D rGO support via electrostatic force to form mesoporous metal–carbon nanosheets.[43] The preformed spherical composite micelles were anchored on a 2D surface, forming a tightly packed monolayer structure. After annealing, they form a functional 2D mesoporous material (Figure 5A). The spherical micelles were attracted to the 2D surface by electrostatic forces (Figure 5B), and dopamine molecules were connected by aggregation between the spherical micelles (Figure 5C).

With rGO@mC-Co-550 as an example, the SEM images revealed that the processed nanosheets retain the 2D structure with a thickness of 36 nm (Figures 6A and 6B), and the TEM image revealed the presence of a large number of spherical mesopores with a diameter of approximately 18 nm (Figure 6F). The thickness of the nanosheets is twice that of the pore size, indicating that the material has formed a double-layer mesoporous structure. Moreover, in the TEM image, it can be seen that the pores partially overlap, further confirming the double-layer

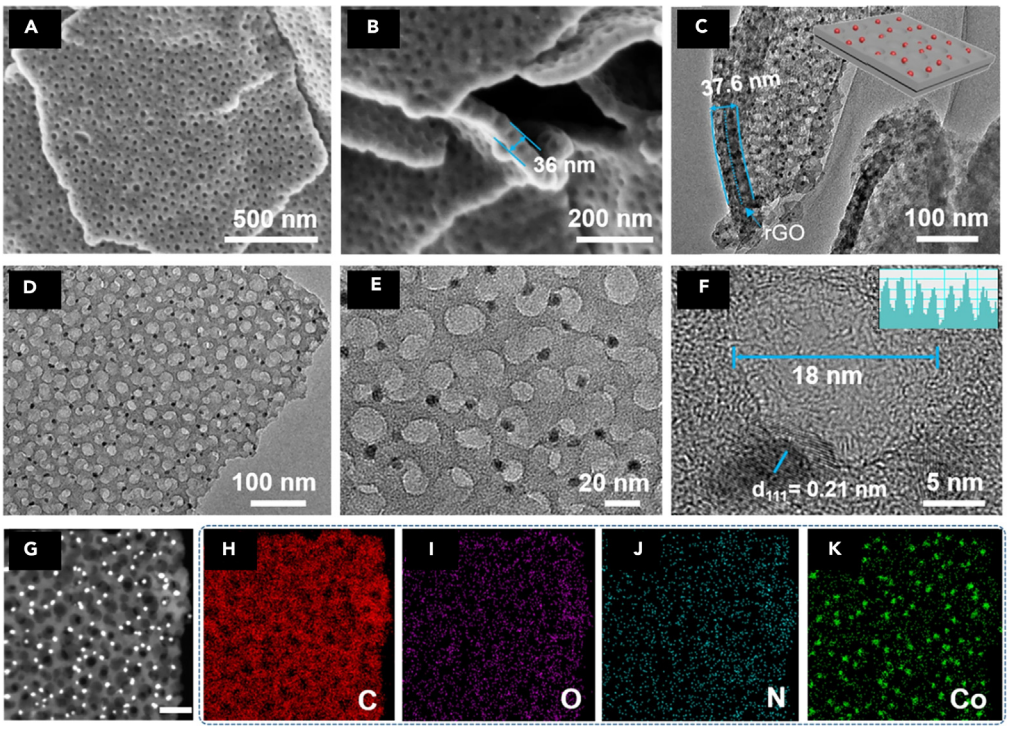

Figure 6. Structure characterization of 2D mesoporous rGO@mC-Co-550 nanosheets

(A and B) SEM, (C–E) TEM, (F) HRTEM, and (G) STEM images of the 2D mesoporous rGO@mC-Co-550 nanosheets; (H–K) EDS elemental mapping spectra of C, O, N, and Co. (G) Scale bar, 50 nm. Reprinted with permission from ref. [43]. Copyright 2023 Springer Nature.

structure (Figures 6D and 6E). The HRTEM images also showed the presence of metal particles with a diameter of approximately 6 nm partially embedded in the pore wall and partially exposed in mesoporous channels. This structure provides an exposed catalytic surface while also avoiding the aggregation of nanoparticles during the reaction.

ORR performance tests were conducted on samples obtained at different annealing temperatures, and it was found that the samples annealed at 850°C had the largest limit current (5.97 mA cm^{-2}) and half-wave potential (0.82 V), which were close to that of commercial Pt/C electrodes (Figure 7A). This catalyst was subjected to cyclic voltammetry testing, and there was no characteristic CV curve in the N_2-saturated solutions. When the electrolyte was switched to an O_2-saturated solution, a conspicuous cathode peak emerged at 0.76 V, which was similar to the cathode peak of Pt/C (Figure 7B). The LSV curves of the material at different rotational speeds were recorded, and the K–L plot showed a prominent linearity. The electron transfer number derived from the K–L plot was 3.6, confirming the $4e^-$ transfer pathway (Figures 7C and 7D). After 5,000 CV cycles, the half-wave potential and current density barely decreased, indicating a good durability (Figure 7E). After the addition of high concentrations of methanol, the current density increased and returned to the original level, whereas the current density for the Pt/C electrode rapidly decreased (Figure 7F). This indicates that the electrode has a strong resistance against methanol and has the potential for application in methanol fuel cells. This synthesis strategy could be used to prepare some 2D model catalysts to probe the reaction mechanism.

Metal-loaded 2D MOF

In 2022, Liu et al. constructed a 2D Ag–Fe–N/C material using ZIF-8 as the precursor through chemical adsorption, calcination, and photodeposition. The resulting material exhibited excellent ORR performance and antibacterial activity, which can promote the efficient and stable operation of microbial fuel cells.[5] First, Fe^{3+} was uniformly adsorbed on the surface of ZIF-8 through chemical adsorption. Subsequently, the zeolite was transformed into an M–N/C structure through high-temperature calcination, retaining some of the pores. Finally, Ag^+ was introduced in these pores and deposited onto the nanosheets via xenon lamp irradiation (Figure 8).

The SEM images showed that after carbonization and photodeposition, the nanosheets still retained their 2D structure, with no significant collapse or agglomeration (Figure 9A). The TEM images showed the presence of nanoparticles and pore structures in the Ag–Fe–N/C-2 material (Figure 9B). The HRTEM image revealed clear lattice fringes in the nanoparticles, with a spacing of 0.233 nm, corresponding to the (111) crystal plane of Ag (Figure 9C). The element mapping image also indicates the uniform distribution of each element (Figure 9D). These data demonstrate the successful preparation of ultra-thin bimetallic nanosheets using this method.

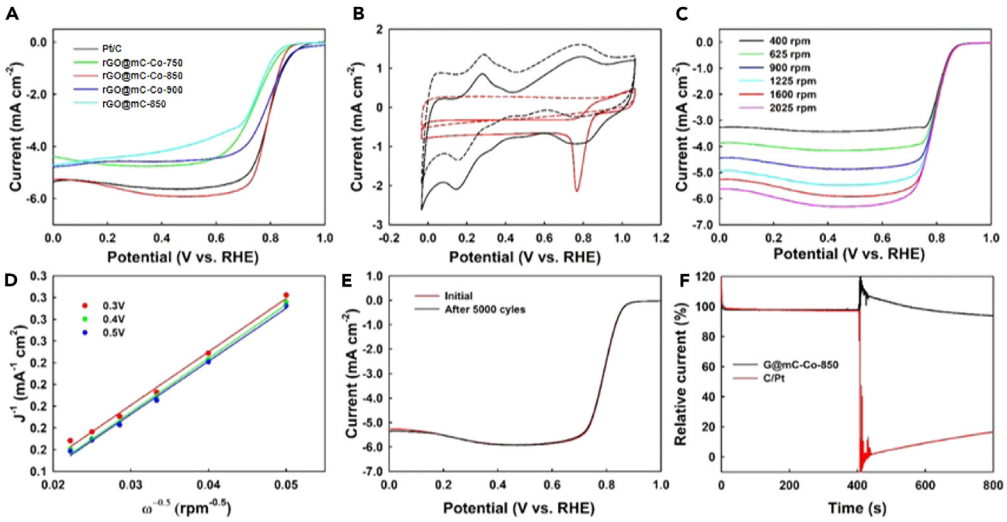

Figure 7. ORR performances of the 2D mesoporous nanosheets

(A) LSV curves of 2D mesoporous nanosheets and Pt/C electrodes obtained with rotation rate of 1600 rpm; (B) CV curves of rGO@mC-Co-850 performed in O_2- and N_2-saturated 0.1 M KOH electrolytes; (C) LSV curves of G@mC-Co-850 obtained at a scan rate of 10 mV s^{-1} with different rotation rates from 400 to 2,025 rpm; (D) K–L plots derived from LSV curves at different electrode potentials; (E) ORR polarization plots for the G@mC-Co-850 before and after 5,000 potential cycles; (F) Current−time (*i*−*t*) chronoamperometric responses of the rGO@mC-Co-850 nanosheets and 20% Pt/C electrodes by adding 20 mL of methanol after 400 s at −0.5 V in O_2-saturated 0.1 M KOH solution. Reprinted with permission from ref. [43]. Copyright 2023 Springer Nature.

LSV tests on Ag–Fe–C/N materials with different Ag loadings unveiled that Ag–Fe–C/N-2 has higher onset potential and half-wave potential than Pt/C, but slightly lower limit current than Pt/C (Figure 10A). Compared with Pt/C, Ag–Fe–C/N-2 has a lower Tafel slope (Figure 10B), which means a lower overpotential. Electrochemical impedance spectroscopy showed that Fe N/C has the lowest charge transfer resistance (R_{ct}), and as the Ag content increases, R_{ct} would gradually increase (Figure 10C). However, R_{ct} is not the only factor affecting the catalytic performance. The C_{dl} curve shows that Ag–Fe–C/N-2 has the largest effective electrochemical surface area (Figure 10D), which is consistent with its best ORR activity. The stability of Ag–Fe–C/N-2 was investigated via chronoamperometry. After continuous operation for 24 h, Ag–Fe–C/N-2 still retained 88% of the initial current density; in contrast, Pt/C deactivated at a faster rate (Figure 10E). The electron transfer number for Ag–Fe–C/N-2 derived from the K–L equation is about 3.90, indicative of the $4e^-$ transfer pathway (Figure 10F).

Hydrogen oxidation reaction

Reaction mechanism

In alkaline media, hydrogen oxidation reaction (HOR) mainly proceeds through the following three steps[53]:

Dissociation of hydrogen molecules:

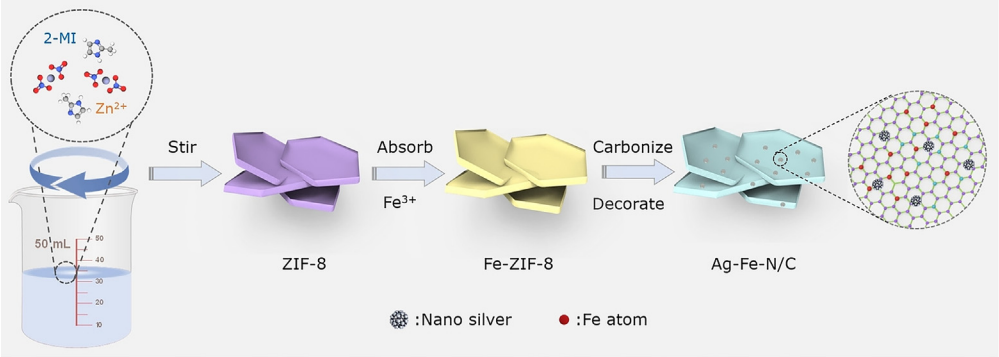

Figure 8. Ag−Fe−N/C preparation process illustration

Reprinted with permission from ref. [5]. Copyright 2022 John Wiley and Sons.

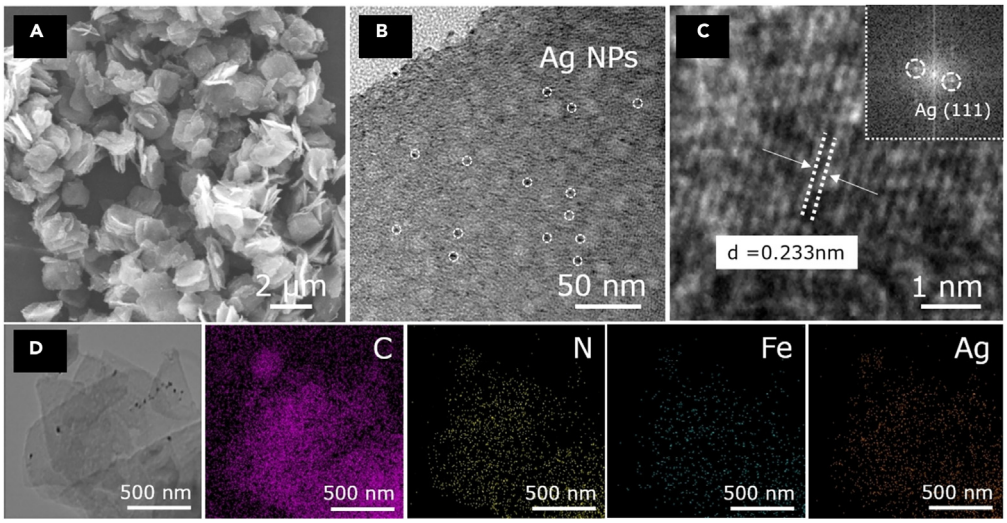

Figure 9. Structure characterization of Ag–Fe–N/C-2

(A) SEM image of Ag–Fe–N/C-2.

(B) TEM image of Ag–Fe–N/C-2.

(C) HRTEM image and FFT pattern of Ag–Fe–N/C-2.

(D) STEM image and elemental mapping of Ag–Fe–N/C-2. Reprinted with permission from ref. [5]. Copyright 2022 John Wiley and Sons.

$$H_2 + 2* \rightarrow 2H_{(ads)} \quad \text{(Equation 12)}$$

Electron transfer from hydrogen molecules to catalysts:

$$H_2 + OH^- + * \rightarrow H_{(ads)} + H_2O + e^- \quad \text{(Equation 13)}$$

Some also believe that the species involved here is $OH_{(ads)}$, so the reaction can be written as:

$$H_2 + OH_{(ads)} \leftrightharpoons H_{(ads)} + H_2O \quad \text{(Equation 14)}$$

$$OH^- + * \rightarrow OH_{(ads)} + e^- \quad \text{(Equation 15)}$$

Releasing H atoms from catalytic center:

$$H_{(ads)} + OH^- \rightarrow * + H_2O + e^- \quad \text{(Equation 16)}$$

2D alloys

Metastable 2D materials have high structural anisotropy and flexible physical and chemical properties and play an important role in catalyst research. However, their thermodynamic instability makes relevant research rather difficult. To enhance the stability of the metastable phase, Zhang et al. synthesized ultra-thin RhMo nanosheets using a one-pot method.[38] During synthesis, $Rh_4(CO)_{12}$, $Mo(CO)_6$, KBr, citric acid monohydrate, and oleamine were simply mixed and sonicated, then heated at 160°C. After washing, RhMo nanosheets were obtained.

The AC-HAADF-STEM image revealed the heterostructure of RhMo alloy. As shown in Figure 11J, the core is composed of the hcp-phase Rh–Mo, whereas the outer shell is composed of a relatively stable fcc-phase Rh–Mo. A clear phase interface could be observed (Figure 11D), and EELS also provided a result of higher Rh content at the outer side (Figure 11F), which supports this fcc@hcp structure.

The polarization curve indicates that RhMo NSs/C has the highest HOR activity, with a current density of 2.99 mA cm^{-2} at 50 mV overpotential (Figure 12A). The polarization curve and K–L equation at different rotational speeds (Figure 12B) were used to confirm the occurrence of a $2e^-$ transfer process. Figure 12C shows the Tafel plots of the kinetic current. The material also has a much higher specific activity than Pt/C (Figure 12D) and other Rh-based or Pt-based electrocatalysts (Figure 12E). Figures 12F and 12G display the polarization curves and peak power density of hydroxide exchange membrane fuel cells for RhMo NSs/C and commercial Pt/C under H_2/O_2 and H_2/air conditions, and it can be seen that RhMo NSs/C has a higher peak power density than commercial Pt/C. In stability tests, the voltage drop was not significant after continuous operation at 0.5A cm^{-2} for 30 h (Figure 12H).

Metal-loaded graphene acid

Graphene acid (GA), a graphene-derived compound with a high content of carboxyl functional groups, can be used to anchor metal sites and is a very attractive support for constructing 2D electrocatalytic materials. It can also be easily obtained from fluorographite. In 2020,

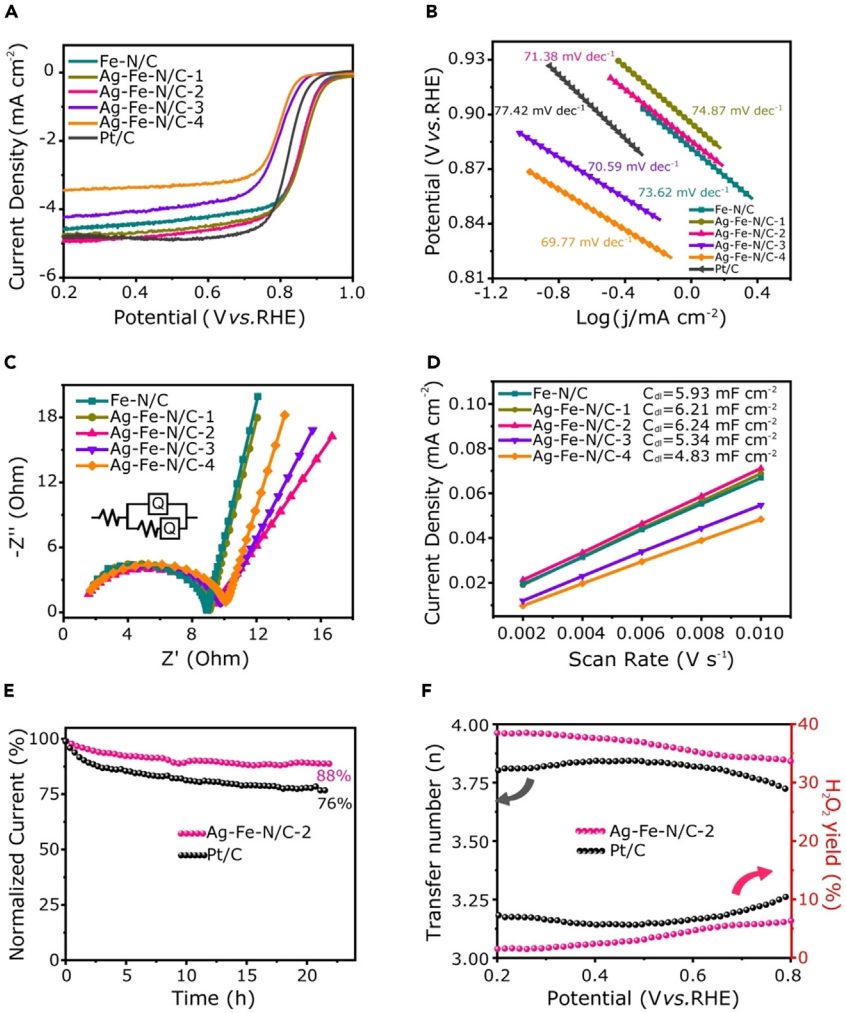

Figure 10. ORR performances of Ag–Fe–N/C-2

(A) LSV curves of catalysts for ORR in O_2-saturated 0.1 M KOH with rotation rate of 1,600 rpm.

(B) Tafel slopes derived from the LSV curves.

(C) Nyquist curves of different catalysts.

(D) Cdl curves of different catalysts.

(E) Chronoamperometric responses in O_2-saturated 0.1 M KOH.

(F) The function between Electron transfer number and H_2O_2 yield versus potential. Reprinted with permission from ref. [5]. Copyright 2022 John Wiley and Sons.

Reuillard et al. developed a biomimetic nickel catalyst that combines with graphene acid through non-covalent bonding to obtain a catalyst for HOR.[6]

This catalyst is assembled through the electrostatic interaction between guanidine salts and carboxyl groups (Figure 13), where graphene acid has carboxyl functional groups with about 10% carbon atoms, which can help anchor a large number of NiArg sites.[3]

The team investigated the relationship between different GA loadings and response current and found an almost linear relationship, and the response current tends to stabilize at 0.4 mgGA cm^{-2} (Figure 14A). At an overvoltage of 0.4 V, the maximum current density can reach 33 mA cm^{-2} (Figure 14B).

CONCLUSION AND PERSPECTIVE

By virtue of their high specific surface areas and flexible structural characteristics, two-dimensional materials have been widely studied in the field of catalysis in recent years. Benefiting from their unique planar structures, the exposure rate of active sites is much higher than that for 3D materials. There are also 2D mesoporous materials such as reduced graphene oxide, which exposes the active sites while

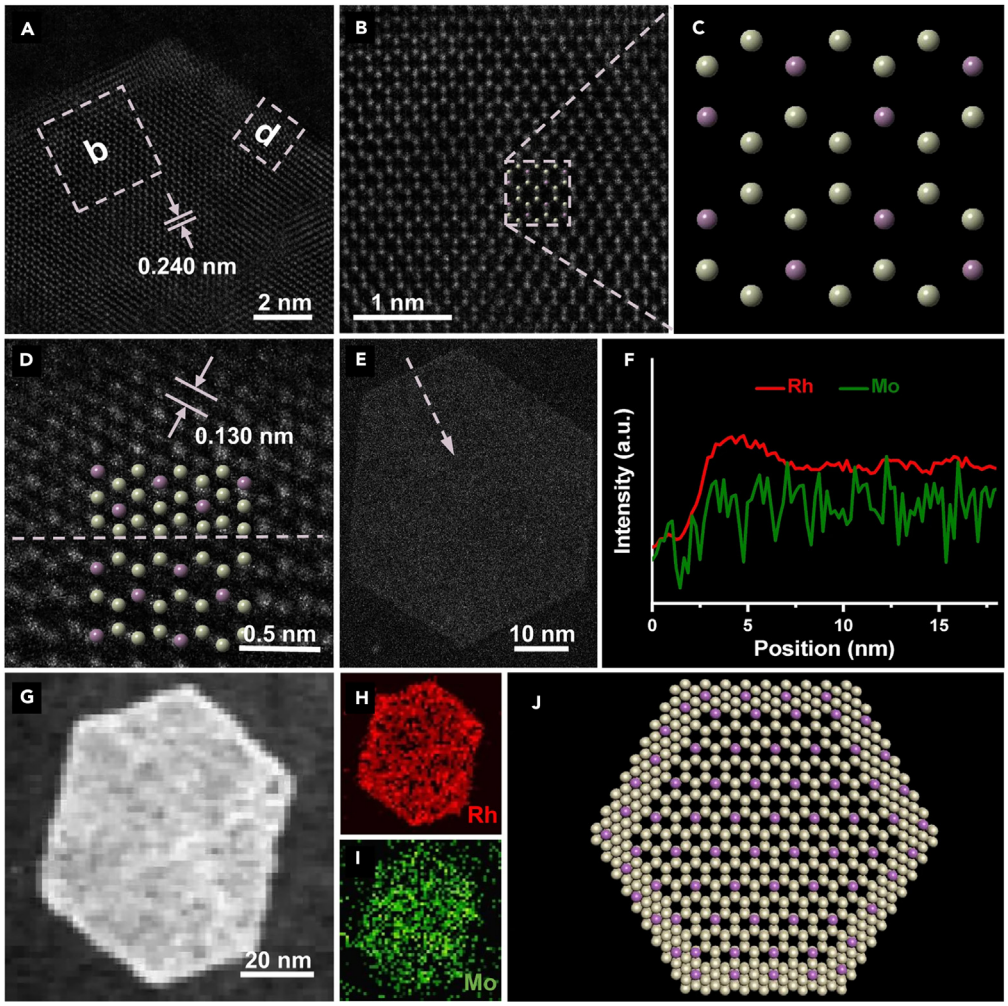

Figure 11. Structure characterization of RhMo NSs

(A) HAADF-STEM image of a single RhMo NS.

(B and D) High-resolution HAADF images of the remarked areas in (A).

(C) Model of atomic arrangement remarked in (B).

(E and F) HAADF-STEM image and corresponding EELS spectroscopy line-scan profiles of a single RhMo NS.

(G–I) STEM-EELS elemental mapping of RhMo NSs: Rh mapping in red and Mo mapping in green.

(J) The schematic illustration of RhMo NSs showing the top view. Atom color code: purple, Mo; white, Rh. Reprinted with permission from ref. [38]. Copyright 2023 Springer Nature.

simultaneously preventing the active species from aggregation. These special characteristics endow 2D materials with great potential for application in fuel cells. Moreover, compared with conventional 3D materials, 2D materials feature a higher utilization of active centers, which could help to lower the cost, energy consumption, and pollution during the preparation process. In this review, we introduce various 2D materials and common synthesis methods developed thus far and discuss their applications for the two simplest electrode reactions in fuel cells, namely, ORR and HOR.

Despite the advantages of 2D materials, their application still faces serious challenges. First, the synthesis of 2D materials is relatively difficult. Currently, the most commonly used solvothermal synthesis method usually affords 2D materials with multiple layers, and the number of layers is uncontrollable. For the exfoliation method, its scope of application is limited because it requires readily available bulk 2D crystals to start with. The CVD method can be used to synthesize most 2D materials, and yet the formation mechanism requires further research; moreover, the CVD fabrication is usually time-consuming and cost-ineffective, and it is therefore difficult to use for large-scale industrial or commercial applications. As a result, more advanced preparation methods need to be developed. Second, although some 2D materials exhibit good stability in the laboratory, the requirements for stability in industry are far more stringent. For example, lithium-ion batteries used in electric vehicles need to work continuously for several years in harsher working environments.

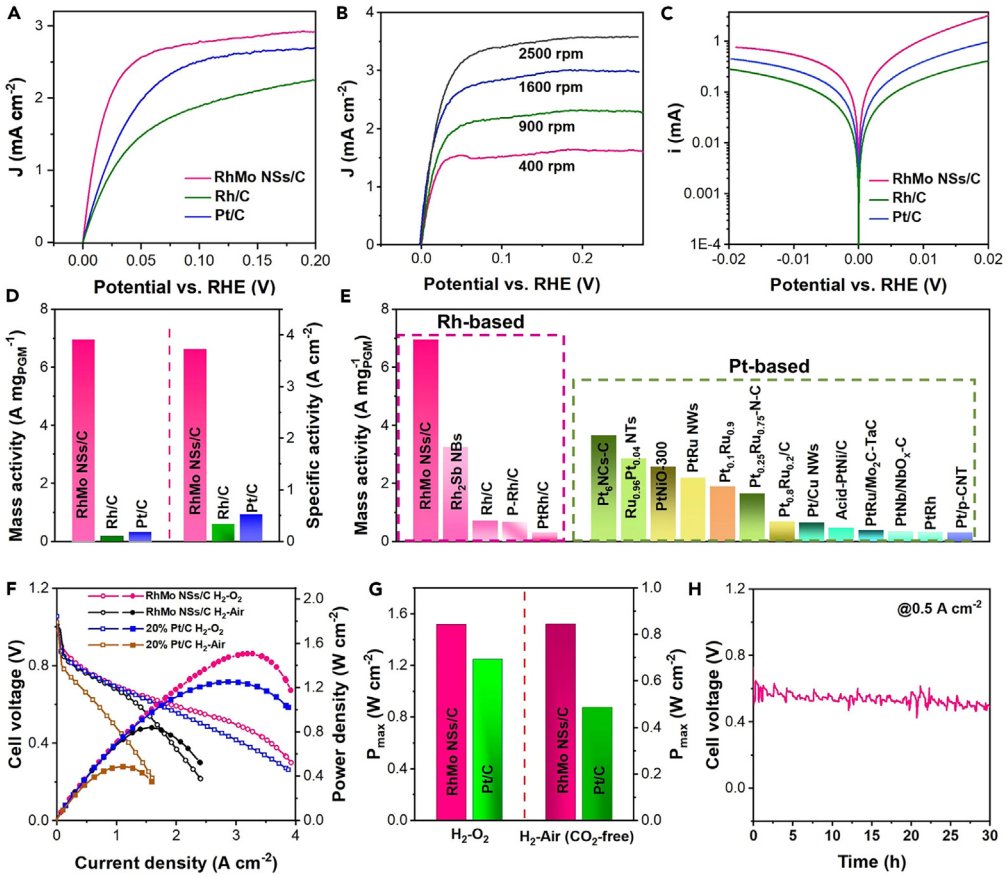

Figure 12. HOR and MEA evaluations of RhMo NSs

(A) HOR polarization curves of RhMo NSs/C, Rh/C, and Pt/C in 0.1 M KOH with a scan rate of 5 mV s^{-1} at a rotation speed of 1,600 rpm.

(B) HOR polarization curves of RhMo NSs/C with different rotation rates from 400 to 2,500 rpm.

(C) Tafel slopes of different catalysts.

(D) Mass activities of RhMo NSs/C, Rh/C, and Pt/C.

(E) Comparison of the mass activity of RhMo NSs/C and previously reported electrocatalysts at an overpotential of 50 mV in 0.1 M KOH.

(F) Polarization curves and peak power density curves of HEMFCs with different catalysts in anode and commercial Pt/C (0.2 mgPt cm^{-2}) in cathode under H_2/O_2 and H_2/air (CO2-free).

(G) The PPDmax of RhMo NSs/C-based and commercial Pt/C-based MEA under H_2–O_2 and H_2/air (CO_2-free) media.

(H) H_2-air/(CO_2-free) HEMFC stability test at the current density of 500 mA cm^{-2} with RhMo NSs/C (0.2 mgRh cm^{-2}) in anode and commercial Pt/C (0.2 mgPt cm^{-2}, 60 wt % Pt/C) in cathode. Reprinted with permission from ref. [38]. Copyright 2023 Springer Nature.

Most 2D materials in the laboratory are incompetent for such a long-time application. Third, precise control over the structures of 2D materials has not yet been achieved, and the synthesis of some 2D materials with special structural characteristics still lacks of sufficient reproducibility. This requires more in-depth research on the growth mechanism of 2D materials. In recent years, more and more *in-situ* characterization techniques have been developed, such as *in-situ* XPS and *in-situ* Raman spectroscopy, which may help to probe their growth mechanisms.

The past decade has witnessed many achievements in 2D materials as an emerging class of advanced catalysts. We believe that with the development of theoretical calculations, experimental characterizations, and preparation techniques, the underlying relationship between structure and performance for 2D materials will be further clarified, and more 2D electrocatalysts will be discovered and applied.

ACKNOWLEDGMENTS

This work was financially supported by the National Key R&D Program of China (2023YFB4005100), National Natural Science Foundation of China (21925202, U22B2071), Yunnan Provincial Science and Technology Project at Southwest United Graduate School (202302AO370017), and International Joint Mission On Climate Change and Carbon Neutrality.

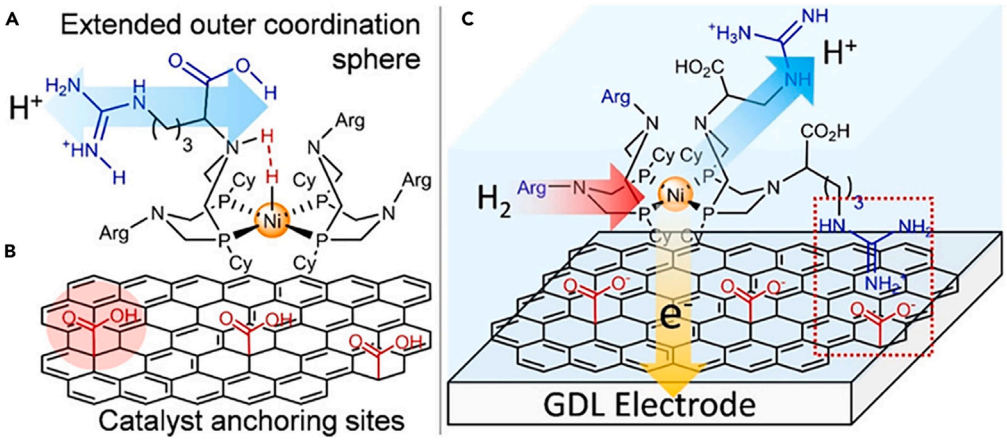

Figure 13. Schematic illustration of NiArg and GA|NiArg

(A) NiArg chemical structure.

(B) GA sheets bearing $-CO_2H$ anchoring functions.

(C) GA|NiArg composite modified electrode. Reprinted with permission from ref. [3]. Copyright 2020 American Chemical Society.

AUTHOR CONTRIBUTIONS

Conceptualization: Z.L. and C.C.; writing–original draft: Z.L. and E.Z.; writing–reviewing & editing: Z.L. and C.Z.; funding acquisition: C.C.; supervision: C.C. and C.Z.

DECLARATION OF INTERESTS

The authors declare no competing interests.

REFERENCES

1. Seh, Z.W., Kibsgaard, J., Dickens, C.F., Chorkendorff, I., Nørskov, J.K., and Jaramillo, T.F. (2017). Combining theory and experiment in electrocatalysis: Insights into materials design. Science *355*, eaad4998. https://doi.org/10.1126/science.aad4998.
2. Simon, P., Gogotsi, Y., and Dunn, B. (2014). Where Do Batteries End and Supercapacitors Begin? Science *343*, 1210–1211. https://doi.org/10.1126/science.1249625.
3. Reuillard, B., Blanco, M., Calvillo, L., Coutard, N., Ghedjatti, A., Chenevier, P., Agnoli, S., Otyepka, M., Granozzi, G., and Artero, V. (2020). Noncovalent Integration of a Bioinspired Ni Catalyst to Graphene Acid for Reversible Electrocatalytic Hydrogen Oxidation. ACS Appl. Mater. Interfaces *12*, 5805–5811. https://doi.org/10.1021/acsami.9b18922.
4. He, C., Zhang, S., and Tao, J. (2022). Two-Dimensional Bimetallic Carbide Boosts Pt toward Oxygen Reduction Reaction. ACS Appl. Energy Mater. *5*, 4382–4389. https://doi.org/10.1021/acsaem.1c03972.
5. Lai, B.-L., Xiao, Z.-H., Jiang, P.-Y., Xie, Y., Li, N., and Liu, Z.-Q. (2022). Two-Dimensional

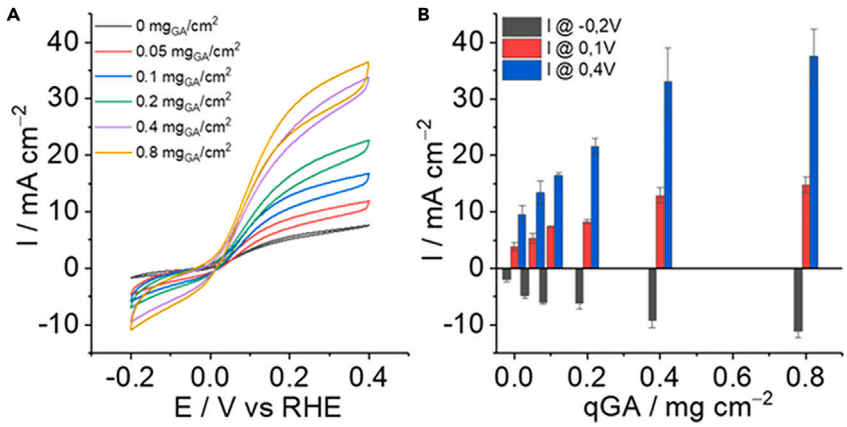

Figure 14. HOR evaluations of GDL|GA electrodes

(A) CV traces of GDL|GA electrodes at various GA loadings modified with 2 μL of NiArg (5 mM).

(B) Current densities for HER at −0.2 V versus RHE and HOR at 0.1 and 0.4 V versus RHE obtained from CVs in 0.5 M H_2SO_4 solution purged with argon with a constant flow of H_2 at the back of the GDL (5 mL min^{-1}) (ν = 20 mV s^{-1}). Reprinted with permission from ref. [3]. Copyright 2020 American Chemical Society.

Ag−Fe−N/C Nanosheets as Efficient Cathode Catalyst to Improve Power-Generation Performance of Microbial Fuel Cells. Chemelectrochem *9*, e202101699. https://doi.org/10.1002/celc.202101699.

6. Novoselov, K.S., Jiang, D., Schedin, F., Booth, T.J., Khotkevich, V.V., Morozov, S.V., and Geim, A.K. (2005). Two-dimensional atomic crystals. Proc. Natl. Acad. Sci. *102*, 10451–10453. https://doi.org/10.1073/pnas.0502848102.
7. Fu, Z., Wang, N., Legut, D., Si, C., Zhang, Q., Du, S., Germann, T.C., Francisco, J.S., and Zhang, R. (2019). Rational Design of Flexible Two-Dimensional MXenes with Multiple Functionalities. Chem. Rev. *119*, 11980–12031. https://doi.org/10.1021/acs.chemrev.9b00348.
8. Ong, W.-J., Tan, L.-L., Ng, Y.H., Yong, S.-T., and Chai, S.-P. (2016). Graphitic Carbon Nitride (g-C3N4)-Based Photocatalysts for Artificial Photosynthesis and Environmental Remediation: Are We a Step Closer To Achieving Sustainability? Chem. Rev. *116*, 7159–7329. https://doi.org/10.1021/acs.chemrev.6b00075.
9. Tan, C., Lai, Z., and Zhang, H. (2017). Ultrathin Two-Dimensional Multinary Layered Metal Chalcogenide Nanomaterials. Adv. Mater. *29*, 1701392. https://doi.org/10.1002/adma.201701392.
10. Yin, H., and Tang, Z. (2016). Ultrathin two-dimensional layered metal hydroxides: an emerging platform for advanced catalysis, energy conversion and storage. Chem. Soc. Rev. *45*, 4873–4891. https://doi.org/10.1039/C6CS00343E.
11. Zheng, Y., Jiao, Y., Zhu, Y., Li, L.H., Han, Y., Chen, Y., Du, A., Jaroniec, M., and Qiao, S.Z. (2014). Hydrogen evolution by a metal-free electrocatalyst. Nat. Commun. *5*, 3783. https://doi.org/10.1038/ncomms4783.
12. Novoselov, K.S., Geim, A.K., Morozov, S.V., Jiang, D., Zhang, Y., Dubonos, S.V., Grigorieva, I.V., and Firsov, A.A. (2004). Electric Field Effect in Atomically Thin Carbon Films. Science *306*, 666–669. https://doi.org/10.1126/science.1102896.
13. Geim, A.K., and Novoselov, K.S. (2007). The rise of graphene. Nat. Mater. *6*, 183–191. https://doi.org/10.1038/nmat1849.
14. Stoller, M.D., Park, S., Zhu, Y., An, J., and Ruoff, R.S. (2008). Graphene-Based Ultracapacitors. Nano Lett. *8*, 3498–3502. https://doi.org/10.1021/nl802558y.
15. Tan, C., Cao, X., Wu, X.-J., He, Q., Yang, J., Zhang, X., Chen, J., Zhao, W., Han, S., Nam, G.-H., et al. (2017). Recent Advances in Ultrathin Two-Dimensional Nanomaterials. Chem. Rev. *117*, 6225–6331. https://doi.org/10.1021/acs.chemrev.6b00558.
16. Jiao, Y., Zheng, Y., Davey, K., and Qiao, S.-Z. (2016). Activity origin and catalyst design principles for electrocatalytic hydrogen evolution on heteroatom-doped graphene. Nat. Energy *1*, 16130. https://doi.org/10.1038/nenergy.2016.130.
17. Xia, C., Qiu, Y., Xia, Y., Zhu, P., King, G., Zhang, X., Wu, Z., Kim, J.Y.T., Cullen, D.A., Zheng, D., et al. (2021). General synthesis of single-atom catalysts with high metal loading using graphene quantum dots. Nat. Chem. *13*, 887–894. https://doi.org/10.1038/s41557-021-00734-x.
18. Jin, H., Guo, C., Liu, X., Liu, J., Vasileff, A., Jiao, Y., Zheng, Y., and Qiao, S.-Z. (2018). Emerging Two-Dimensional Nanomaterials for Electrocatalysis. Chem. Rev. *118*, 6337–6408. https://doi.org/10.1021/acs.chemrev.7b00689.
19. Ma, T.Y., Ran, J., Dai, S., Jaroniec, M., and Qiao, S.Z. (2015). Phosphorus-Doped Graphitic Carbon Nitrides Grown In Situ on Carbon-Fiber Paper: Flexible and Reversible Oxygen Electrodes. Angew. Chem., Int. Ed. *54*, 4646–4650. https://doi.org/10.1002/anie.201411125.
20. Jaramillo, T.F., Jørgensen, K.P., Bonde, J., Nielsen, J.H., Horch, S., and Chorkendorff, I. (2007). Identification of Active Edge Sites for Electrochemical H2 Evolution from MoS2 Nanocatalysts. Science *317*, 100–102. https://doi.org/10.1126/science.1141483.
21. Chhowalla, M., Shin, H.S., Eda, G., Li, L.-J., Loh, K.P., and Zhang, H. (2013). The chemistry of two-dimensional layered transition metal dichalcogenide nanosheets. Nat. Chem. *5*, 263–275. https://doi.org/10.1038/nchem.1589.
22. Kalantar-zadeh, K., Ou, J.Z., Daeneke, T., Mitchell, A., Sasaki, T., and Fuhrer, M.S. (2016). Two dimensional and layered transition metal oxides. App. Mater. Today *5*, 73–89. https://doi.org/10.1016/j.apmt.2016.09.012.
23. Xu, L., Jiang, Q., Xiao, Z., Li, X., Huo, J., Wang, S., and Dai, L. (2016). Plasma-Engraved Co3 O4 Nanosheets with Oxygen Vacancies and High Surface Area for the Oxygen Evolution Reaction. Angew. Chem. Int. Ed. Engl. *55*, 5277–5281. https://doi.org/10.1002/anie.201600687.
24. Qian, L., Lu, Z., Xu, T., Wu, X., Tian, Y., Li, Y., Huo, Z., Sun, X., and Duan, X. (2015). Trinary Layered Double Hydroxides as High-Performance Bifunctional Materials for Oxygen Electrocatalysis. Adv. Energy Mater. *5*, 1500245. https://doi.org/10.1002/aenm.201500245.
25. Naguib, M., Kurtoglu, M., Presser, V., Lu, J., Niu, J., Heon, M., Hultman, L., Gogotsi, Y., and Barsoum, M.W. (2011). Two-Dimensional Nanocrystals Produced by Exfoliation of Ti3AlC2. Adv. Mater. *23*, 4248–4253. https://doi.org/10.1002/adma.201102306.
26. Gao, L., Li, C., Huang, W., Mei, S., Lin, H., Ou, Q., Zhang, Y., Guo, J., Zhang, F., Xu, S., and Zhang, H. (2020). MXene/Polymer Membranes: Synthesis, Properties, and Emerging Applications. Chem. Mater. *32*, 1703–1747. https://doi.org/10.1021/acs.chemmater.9b04408.
27. Zhang, J., Zhao, Y., Guo, X., Chen, C., Dong, C.-L., Liu, R.-S., Han, C.-P., Li, Y., Gogotsi, Y., and Wang, G. (2018). Single platinum atoms immobilized on an MXene as an efficient catalyst for the hydrogen evolution reaction. Nat. Catal. *1*, 985–992. https://doi.org/10.1038/s41929-018-0195-1.
28. Wang, M., Zhu, J., Zi, Y., Wu, Z.-G., Hu, H., Xie, Z., Zhang, Y., Hu, L., and Huang, W. (2021). Functional two-dimensional black phosphorus nanostructures towards next-generation devices. J. Mater. Chem. A *9*, 12433–12473. https://doi.org/10.1039/D1TA02027G.
29. Xie, Z., Zhang, B., Ge, Y., Zhu, Y., Nie, G., Song, Y., Lim, C.-K., Zhang, H., and Prasad, P.N. (2022). Chemistry, Functionalization, and Applications of Recent Monoelemental Two-Dimensional Materials and Their Heterostructures. Chem. Rev. *122*, 1127–1207. https://doi.org/10.1021/acs.chemrev.1c00165.
30. Wang, M., Hu, Y., Pu, J., Zi, Y., and Huang, W. (2024). Emerging Xene-Based Single-Atom Catalysts: Theory, Synthesis, and Catalytic Applications. Adv. Mater. *36*, 2303492. https://doi.org/10.1002/adma.202303492.
31. Huang, W., Zhu, J., Wang, M., Hu, L., Tang, Y., Shu, Y., Xie, Z., and Zhang, H. (2021). Emerging Mono-Elemental Bismuth Nanostructures: Controlled Synthesis and Their Versatile Applications. Adv. Funct. Mater. *31*, 2007584. https://doi.org/10.1002/adfm.202007584.
32. Huang, W., Zhu, J., Wang, M., Hu, L., Tang, Y., Shu, Y., Xie, Z., and Zhang, H. (2021). Emerging Mono-Elemental Bismuth Nanostructures: Controlled Synthesis and Their Versatile Applications. Adv. Funct. Mater. *31*, 2007584. https://doi.org/10.1002/adfm.202007584.
33. Wang, W., Xu, X., Zhou, W., and Shao, Z. (2017). Recent Progress in Metal-Organic Frameworks for Applications in Electrocatalytic and Photocatalytic Water Splitting. Adv. Sci. *4*, 1600371. https://doi.org/10.1002/advs.201600371.
34. Zhao, S., Wang, Y., Dong, J., He, C.-T., Yin, H., An, P., Zhao, K., Zhang, X., Gao, C., Zhang, L., et al. (2016). Ultrathin metal–organic framework nanosheets for electrocatalytic oxygen evolution. Nat. Energy *1*, 16184. https://doi.org/10.1038/nenergy.2016.184.
35. Kornienko, N., Zhao, Y., Kley, C.S., Zhu, C., Kim, D., Lin, S., Chang, C.J., Yaghi, O.M., and Yang, P. (2015). Metal–Organic Frameworks for Electrocatalytic Reduction of Carbon Dioxide. J. Am. Chem. Soc. *137*, 14129–14135. https://doi.org/10.1021/jacs.5b08212.
36. Rodenas, T., Luz, I., Prieto, G., Seoane, B., Miro, H., Corma, A., Kapteijn, F., Llabrés i Xamena, F.X., and Gascon, J. (2015). Metal–organic framework nanosheets in polymer composite materials for gas separation. Nat. Mater. *14*, 48–55. https://doi.org/10.1038/nmat4113.
37. Chen, Y., Ji, S., Wang, Y., Dong, J., Chen, W., Li, Z., Shen, R., Zheng, L., Zhuang, Z., Wang, D., and Li, Y. (2017). Isolated Single Iron Atoms Anchored on N-Doped Porous Carbon as an Efficient Electrocatalyst for the Oxygen Reduction Reaction. Angew. Chem., Int. Ed. *56*, 6937–6941. https://doi.org/10.1002/anie.201702473.
38. Zhang, J., Liu, X., Ji, Y., Liu, X., Su, D., Zhuang, Z., Chang, Y.-C., Pao, C.-W., Shao, Q., Hu, Z., and Huang, X. (2023). Atomic-thick metastable phase RhMo nanosheets for hydrogen oxidation catalysis. Nat. Commun. *14*, 1761. https://doi.org/10.1038/s41467-023-37406-y.
39. Joensen, P., Frindt, R.F., and Morrison, S. (1986). Single-layer MoS2. Mater. Res. Bull. *21*, 457–461. https://doi.org/10.1016/0025-5408(86)90011-5.
40. Pollard, A.J., Nair, R.R., Sabki, S.N., Staddon, C.R., Perdigao, L.M.A., Hsu, C.H., Garfitt, J.M., Gangopadhyay, S., Gleeson, H.F., Geim, A.K., and Beton, P.H. (2009). Formation of Monolayer Graphene by Annealing Sacrificial Nickel Thin Films. J. Phys. Chem. C *113*, 16565–16567. https://doi.org/10.1021/jp906066z.
41. Sun, Z., Liao, T., Dou, Y., Hwang, S.M., Park, M.-S., Jiang, L., Kim, J.H., and Dou, S.X. (2014). Generalized self-assembly of scalable two-dimensional transition metal oxide nanosheets. Nat. Commun. *5*, 3813. https://doi.org/10.1038/ncomms4813.
42. Tang, Z., Zhang, Z., Wang, Y., Glotzer, S.C., and Kotov, N.A. (2006). Self-Assembly of CdTe Nanocrystals into Free-Floating Sheets. Science *314*, 274–278. https://doi.org/10.1126/science.1128045.

43. Qiu, P., Zhang, X., Ai, Y., Luo, W., Li, W., and Zhao, D. (2023). Modular assembly of metal nanoparticles/mesoporous carbon two-dimensional nanosheets. NPG Asia Mater. *15*, 35. https://doi.org/10.1038/s41427-023-00482-z.
44. Cheng, W., Lu, X.F., Luan, D., and Lou, X.W.D. (2020). NiMn-Based Bimetal–Organic Framework Nanosheets Supported on Multi-Channel Carbon Fibers for Efficient Oxygen Electrocatalysis. Angew. Chem., Int. Ed. *59*, 18234–18239. https://doi.org/10.1002/anie.202008129.
45. Gao, R., Yin, Y., Niu, F., Wang, A., Li, S., Dong, H., and Yang, S. (2019). One Pot Synthesis of FeCo/N-Doped 3D Porous Carbon Nanosheets as Bifunctional Electrocatalyst for the Oxygen Reduction and Evolution Reactions. Chemelectrochem *6*, 1824–1830. https://doi.org/10.1002/celc.201900016.
46. Liu, J., He, T., Wang, Q., Zhou, Z., Zhang, Y., Wu, H., Li, Q., Zheng, J., Sun, Z., Lei, Y., et al. (2019). Confining ultrasmall bimetallic alloys in porous N–carbon for use as scalable and sustainable electrocatalysts for rechargeable Zn–air batteries. J. Mater. Chem. A *7*, 12451–12456. https://doi.org/10.1039/C9TA02264C.
47. Strmcnik, D., Uchimura, M., Wang, C., Subbaraman, R., Danilovic, N., van der Vliet, D., Paulikas, A.P., Stamenkovic, V.R., and Markovic, N.M. (2013). Improving the hydrogen oxidation reaction rate by promotion of hydroxyl adsorption. Nat. Chem. *5*, 300–306. https://doi.org/10.1038/nchem.1574.
48. Wang, X., Zhao, L., Li, X., Liu, Y., Wang, Y., Yao, Q., Xie, J., Xue, Q., Yan, Z., Yuan, X., and Xing, W. (2022). Atomic-precision Pt6 nanoclusters for enhanced hydrogen electro-oxidation. Nat. Commun. *13*, 1596. https://doi.org/10.1038/s41467-022-29276-7.
49. Huang, Z., Hu, S., Sun, M., Xu, Y., Liu, S., Ren, R., Zhuang, L., Chan, T.-S., Hu, Z., Ding, T., et al. (2024). Implanting oxophilic metal in PtRu nanowires for hydrogen oxidation catalysis. Nat. Commun. *15*, 1097. https://doi.org/10.1038/s41467-024-45369-x.
50. Zhao, G., Xia, L., Cui, P., Qian, Y., Jiang, Y., Zhao, Y., Pan, H., Dou, S.X., and Sun, W. (2021). Atomic-Level Modulation of the Interface Chemistry of Platinum–Nickel Oxide toward Enhanced Hydrogen Electrocatalysis Kinetics. Nano Lett. *21*, 4845–4852. https://doi.org/10.1021/acs.nanolett.1c01519.
51. Yu, L., Pan, X., Cao, X., Hu, P., and Bao, X. (2011). Oxygen reduction reaction mechanism on nitrogen-doped graphene: A density functional theory study. J. Catal. *282*, 183–190. https://doi.org/10.1016/j.jcat.2011.06.015.
52. Chai, G.-L., Hou, Z., Ikeda, T., and Terakura, K. (2017). Two-Electron Oxygen Reduction on Carbon Materials Catalysts: Mechanisms and Active Sites. J. Phys. Chem. C *121*, 14524–14533. https://doi.org/10.1021/acs.jpcc.7b04959.
53. Davydova, E.S., Mukerjee, S., Jaouen, F., and Dekel, D.R. (2018). Electrocatalysts for Hydrogen Oxidation Reaction in Alkaline Electrolytes. ACS Catal. *8*, 6665–6690. https://doi.org/10.1021/acscatal.8b00689.